Published September 1, 1992

Gating of O_2-sensitive K^+ Channels of Arterial Chemoreceptor Cells and Kinetic Modifications Induced by Low P_{O_2}

MARÍA DOLORES GANFORNINA and JOSÉ LÓPEZ-BARNEO

From the Departamento de Fisiología y Biofísica, Facultad de Medicina, Universidad de Sevilla, 41009 Sevilla, Spain

ABSTRACT We have studied the kinetic properties of the O_2-sensitive K^+ channels (K_{O_2} channels) of dissociated glomus cells from rabbit carotid bodies exposed to variable O_2 tension (P_{O_2}). Experiments were done using single-channel and whole-cell recording techniques. The major gating properties of K_{O_2} channels in excised membrane patches can be explained by a minimal kinetic scheme that includes several closed states (C_0 to C_4), an open state (O), and two inactivated states (I_0 and I_1). At negative membrane potentials most channels are distributed between the left-most closed states (C_0 and C_1), but membrane depolarization displaces the equilibrium toward the open state. After opening, channels undergo reversible transitions to a short-living closed state (C_4). These transitions configure a burst, which terminates by channels either returning to a closed state in the activation pathway (C_3) or entering a reversible inactivated conformation (I_0). Burst duration increases with membrane depolarization. During a maintained depolarization, K_{O_2} channels make several bursts before ending at a nonreversible, absorbing, inactivated state (I_1). On moderate depolarizations, K_{O_2} channels inactivate very often from a closed state. Exposure to low P_{O_2} reversibly induces an increase in the first latency, a decrease in the number of bursts per trace, and a higher occurrence of closed-state inactivation. The open state and the transitions to adjacent closed or inactivated states seem to be unaltered by hypoxia. Thus, at low P_{O_2} the number of channels that open in response to a depolarization decreases, and those channels that follow the activation pathway open more slowly and inactivate faster. At the macroscopic level, these changes are paralleled by a reduction in the peak current amplitude, slowing down of the activation kinetics, and acceleration of the inactivation time course. The effects of low P_{O_2} can be explained by assuming that under this condition the closed state C_0 is stabilized and the transitions to the absorbing inactivated state I_1 are favored. The fact that hypoxia modifies kinetically defined conformational states of the channels suggests that O_2 levels determine the structure of specific domains of the K_{O_2} channel molecule. These results help to understand the molecular mechanisms underlying the enhancement of the excitability of glomus cells in response to hypoxia.

Address reprint requests to Dr. José López-Barneo, Departamento de Fisiología y Biofisíca, Facultad de Medicina, Avenida Sánchez Pizjuán, 4, 41009 Sevilla, Spain.

J. GEN. PHYSIOL. © The Rockefeller University Press · 0022-1295/92/09/0427/29 $2.00 427
Volume 100 September 1992 427–455

INTRODUCTION

Recent electrophysiological studies on type I (or glomus) cells of the mammalian carotid body have shown that they can generate action potentials due to the activity of voltage-gated Na^+, Ca^{2+}, and K^+ channels of their plasma membrane (Duchen, Caddy, Kirby, Patterson, Ponte, and Biscoe, 1988; López-Barneo, López-López, Ureña, and González, 1988; Hescheler, Delpiano, Acker, and Pietruschka, 1989; Ureña, López-López, González, and López-Barneo, 1989), and that low environmental O_2 tension (Po_2) produces a selective and reversible attenuation of the K^+ current (López-Barneo et al., 1988; Delpiano and Hescheler, 1989; López-López, González, Ureña, and López-Barneo, 1989; Stea and Nurse, 1991). These electrophysiological findings have opened new perspectives on the physiology of the carotid body and provided a deeper understanding of the mechanisms responsible for the chemosensory properties of type I cells. Inhibition of the K^+ current in response to low Po_2 produces an increase in the firing frequency of the cells which may lead to Ca^{2+} entry and enhanced release of the transmitters that activate the afferent fibers of the sinus nerve (López-López et al., 1989).

The present experiments were designed to address two major questions: (*a*) Can O_2 interact with a specific type of K^+ channel in a manner that would account for the modulation of the macroscopic K^+ current? If so, (*b*) what modifications in channel gating are induced by altering O_2? In the preceding article (Ganfornina and López-Barneo, 1992) we have reported the existence of three major classes of voltage-activated K^+ channels in glomus cells and shown that changes in Po_2 modulate the activity of only one type, referred to as the K_{O_2} channel. The experimental data indicate that low Po_2 decreases single-channel open probability and suggest that O_2 may act through a sensor intrinsic to the membrane closely associated with the channel protein. Thus, the unique characteristics of K_{O_2} channels explain the effect of altering Po_2 on the electrical properties of glomus cells.

In this article we have aimed at a more detailed and quantitative study of the gating kinetics of K_{O_2} channels by the combined analysis of single-channel and macroscopic currents. Voltage-gated K^+ channels are extraordinarily diverse and appear to be expressed in many different cell types (for review, see Rudy, 1988), but detailed, nonstationary kinetic analysis has been done in only a few preparations (see Hoshi and Aldrich, 1988; Cooper and Shrier, 1989; Solc and Aldrich, 1990; Zagotta and Aldrich, 1990). These channels, although primarily regulated by changes in the transmembrane electric field, can be modulated by a number of ions, metabolites, and enzymes (for review, see Levitan, 1988). The interaction of modulators with K^+ channels and the precise changes induced in their gating properties are, however, poorly studied and far from being understood (see Perozo, Jong, and Bezanilla, 1991). Here we propose a kinetic scheme including the minimal conformational states required to explain the basic gating properties of K_{O_2} channels. The model is based on sequential state diagrams of inactivating Na^+ and K^+ channels (see, for example, Armstrong and Bezanilla, 1977; Armstrong and Gilly, 1979; Aldrich, Corey, and Stevens, 1983; Zagotta and Aldrich, 1990) and it provides the conceptual framework necessary for organizing and understanding the effect of O_2 on channel function. Our results suggest that the effects of low Po_2 can be explained by

stabilization of kinetically defined conformational states of the K_{O_2} channels, which may indicate that changes in P_{O_2} induce structural modifications in specific domains of the channel molecule.

METHODS

Culture and Recording Techniques

Details of the methodology used appear in the preceding paper (Ganfornina and López-Barneo, 1992). Enzymatic dispersion of the cells and recording were performed using techniques described previously (see Ureña et al., 1989). For whole-cell and single-channel recording we used the different variants of the patch clamp technique (Hamill, Marty, Neher, Sakmann, and Sigworth, 1981). Digitized records were corrected for linear leakage and uncompensated capacity currents before analysis. Solutions, indicated as external//internal, as well as the protocol followed to test the effect of low P_{O_2} on the properties of single-channel and whole-cell currents were the same as in the preceding paper. All experiments were conducted at room temperature (22–25°C).

Analysis

Macroscopic whole-cell currents and the ensemble averages obtained from original single-channel current traces were analyzed following standard procedures. The final frequency response of the cascade of Bessel filters used (patch clamp and filter) was characterized, at different cutoff frequencies, by the rise time (T_r) of the output signal when a square wave was applied at the input. T_r was used afterwards to impose a resolution to the measurements of duration and amplitude of single-channel events. Amplitude of unitary currents was measured only for openings of duration $\geq 2 \cdot T_r$. We used a 50% threshold-crossing method to detect opening and closing transitions and a resolution of $1.3 \cdot T_r$ was subsequently imposed on the interval duration as indicated by Colquhoun and Sigworth (1983; see also Colquhoun, 1988). The effective cutoff frequency, the resolution imposed on the data, and the digitizing sample interval used in each experiment are indicated in the figure legends. Unless otherwise noted, no correction for unresolved events was performed.

All the data used for the calculations of this paper were obtained during depolarizing pulses. In all experiments the interval between test pulses was at least 30 s to avoid cumulative inactivation. We have measured the duration of open and closed events, first latency, and burst length, as well as the number of bursts per trace. Because even with small pipettes the probability of finding a patch with only one or two K_{O_2} channels is very low, and, in addition, these channels recover from inactivation very slowly (which prevents the acquisition of a large number of stable recordings in a reasonable period of time), the number of events was relatively small in some of the time interval distributions studied. To minimize this limitation, open time, closed time, and burst length distributions were fitted with probability density functions (pdf) with one or the sum of several exponential terms by the method of maximum likelihood. This method of fitting a variable takes into account each one of the individual measurements and thus gives a more sensible estimate than other methods where the data are grouped into bins (Colquhoun and Sigworth, 1983). We used the conditional pdf, $f(t)$, given that it is restricted to a range between t_{min} and t_{max} (see Colquhoun and Hawkes, 1983; Colquhoun and Sigworth, 1983). For the graphic representation of the data, closed and open time as well as burst duration were displayed as cumulative histograms and the scaled function $g(t) = 1 - F(t)$ (where $F(t)$ is a distribution function integral of pdf) was superimposed on them. The number of events in each distribution is given in the figure legends. First latency distributions were displayed as a cumulative histogram and a distribution function was fitted to the data by a

least-squares method. The number of bursts per trace was fitted to the sum of one or more geometric terms by the maximum likelihood method. Distributions were fitted by several pdf or distribution functions with a different number of exponential terms or unknown parameters. In all instances, the extent to which a model with more parameters improved the fit was evaluated with a likelihood ratio test as described by Horn (1987).

Most kinetic parameters were estimated in patches with only one channel, although occasionally first latency and open time distributions were also estimated in patches containing two channels (the number of channels in a patch was estimated as indicated in the preceding paper). In these cases, the true first latency distribution was obtained after correction for the number of channels as indicated by Patlak and Horn (1982). When the opening of two channels overlapped, we assumed that the channel that opened first closed first 50% of the times (Aldrich et al., 1983; Cooper and Shrier, 1989). In patches with more than one channel the true probability of the occurrence of records that had no openings (blank records) was taken as the Nth root of the apparent probability (Aldrich et al., 1983).

When appropriate, significance of differences between mean values obtained in different experimental conditions was determined with a Student's t test for paired samples. The nonparametric Mann-Whitney U test was used to compare data distributions. The Spearman coefficient (r_s) was used to test the existence of correlation between random variables. Unless indicated otherwise, the significance level (α) of the tests was set at 0.05.

RESULTS

Gating of K_{O_2} Channels

Channels traverse several closed states during activation. Activation of the K_{O_2} channels follows a sigmoidal time course with an initial delay, which suggests that they must traverse more than one closed state before opening. Fig. 1 shows the time course of the macroscopic O_2-sensitive K^+ current (top), the ensemble average current from an outside-out patch with at least four K_{O_2} channels (middle), and the cumulative first latency distribution in an inside-out patch with one K_{O_2} channel (bottom). This distribution illustrates that upon step depolarization the channel opens with a variable lag (depicted in the inset to the figure) and specifies the probability that the first channel opening (ordinate) occurred at time $\leq t$ (abscissa) since the onset of the pulse. The traces reveal that the time courses of the whole-cell and the ensemble average currents are almost identical and comparable to the shape of the first latency histogram. Macroscopic and ensemble average currents reach half-maximal amplitude ($t_{1/2}$) in 1.1 and 1.4 ms, respectively, which are values quite similar to the time at which the first latency distribution crosses 50% of its maximum value (median first latency = 1.2 ms). In the cumulative first latency distribution probability does not reach unity because some pulses had no channel openings (blank traces). Since blank sweeps were observed even during pulses lasting up to 3 s (a time period clearly larger than the longest latency observed) it can be hypothesized, in accordance with previous work in other channel types (Horn, Patlak, and Stevens, 1981; Hoshi and Aldrich, 1988; Cooper and Shrier, 1989), that K_{O_2} channels undergo direct conformational transitions from closed to inactivated states without traversing the open state, or that they are inactivated with ~20% probability before the pulse.

Transitions to the open state are voltage dependent. The number of closed states leading to the open state and the value of the rate constants characterizing transitions among states were estimated in two steps. First, we evaluated the number

Published September 1, 1992

of states in the activation pathway by fitting a distribution function with several exponential terms to cumulative first latency histograms obtained at various membrane potentials. For simplicity the fitting was done on the basis of several assumptions summarized in Scheme 1.

$$C_0 \xrightarrow{k} C_1 \xrightarrow{3\alpha} C_2 \xrightarrow{2\alpha} C_3 \xrightarrow{\alpha} O$$

SCHEME 1

It is proposed that transitions from state C_1 to the open state (O) come about by the independent movement of three identical charges. This constrains rate constants

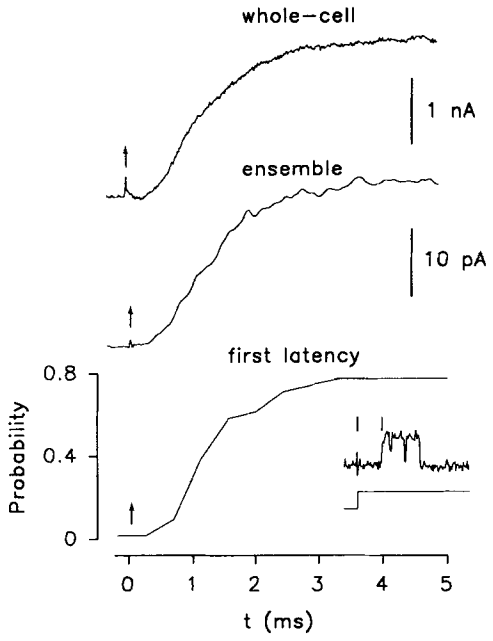

FIGURE 1. Activation time course of the macroscopic O_2-sensitive K^+ current and K_{O_2} channels. Macroscopic K^+ current (*top*), ensemble average current (20 pulses) from an outside-out patch with at least four K_{O_2} channels (*middle*), and cumulative first latency distribution from an inside-out patch with $N = 1$ K_{O_2} channel (*bottom*). In all cases pulses were applied from −80 to +20 mV and time was measured from the onset of the pulse (*arrows*). Solutions: standard Na, TTX//standard K, 10 EGTA (*top and middle*) and standard Na, TTX//130 K, 10 EGTA (*bottom*).

for transitions to be integer multiples of the voltage-dependent first order transition rate α, and therefore reduces the number of parameters that must be determined. We also supposed that at positive membrane potentials the deactivation rate constant (β) can be neglected and that at resting all the channels are in state C_0. Thus, the C_0 to C_1 transition is characterized by an unconstrained first order rate constant (*k*) which was assumed to be independent of voltage. This model fitted the data significantly better than the ones with fewer states, as well as models where the rate constant *k* was made voltage dependent and a multiple of α (4α) or all the rate constants were unconstrained. Moreover, it provided a simpler explanation for the effects of low P_{O_2}. As shown in another section, hypoxia slows down the activation kinetics of K_{O_2} channels without altering the transitions adjacent to the open state. Hence, it was conceived as likely that at negative membrane potentials K_{O_2} channels are distributed

between states C_0 and C_1 and that transitions between these states are regulated by P_{O_2}.

A final estimate of the rate constants in the opening pathway was done by fitting to cumulative first latency histograms the numerical solutions of the state diagram represented in Scheme 2.

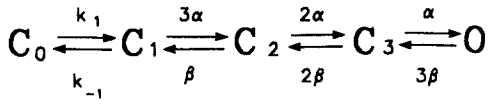

SCHEME 2

The voltage-independent rate constants k_1 and k_{-1} were chosen such as to determine that at resting and under normoxic conditions 97.5% of the channels are in state C_1, and the value of the rate constant α calculated with the constraint that β, estimated from the fitting to the voltage dependence of the burst duration (see Fig. 4 *C*, below), was set to 32 s^{-1} at 0 mV. Fig. 2 *A* shows first latency histograms obtained during depolarizations to various membrane potentials. The fittings obtained following Scheme 2 scaled by the number of blanks observed at each membrane potential are superimposed. The data illustrate the shortening of the median first latency with depolarization as a result of the opposite voltage dependence of the rate constants α and β. The values of α (filled symbols) and β (open symbols) estimated at different membrane potentials are plotted in Fig. 2 *B*. The solid lines follow the exponential equations:

$$\alpha(V) = A_\alpha \cdot e(V/V_\alpha) \quad (1)$$

$$\beta(V) = A_\beta \cdot e^{-}(V/V_\beta) \quad (2)$$

where A_α and A_β are the values of α and β at 0 mV (201 and 32 s^{-1}, respectively), and V_α (22 mV) and V_β (21 mV) are slope constants specifying the membrane potential displacement required for an *e*-fold increase or reduction of α and β, respectively. Matching of the model to experimental findings is further shown in Fig. 2 *C*, where it is illustrated that ensemble averages of single K_{O_2} channel currents recorded at various membrane potentials have a rising phase comparable to the theoretical fits plotted in Fig. 2 *A* (compare also traces in Fig. 1, *B* and *C*). In these records half-time to peak current also varies exponentially with the membrane potential with a slope constant of −12 mV (Fig. 2 *D*).

Closed interval distribution. During a step depolarization, K_{O_2} channels exhibit, after the first opening, several open/closed transitions, with distinct closed intervals separating consecutive openings. These intervals, tentatively grouped into three major categories, are illustrated in Fig. 3 *A* by representative recordings obtained from a patch with one channel. Open periods were interrupted by fast transitions to a nonconducting state with a lifetime of only a few hundred microseconds (single asterisks). The occurrence of these brief closed events was surely underestimated because most transitions could have been partially, or totally, filtered due to the limited recording bandwidth. Fast open/closed transitions were defined as within a "burst" following a burst criterion duration (Magleby and Pallota, 1983). We set the

burst criterion at 2.5 ms (five times the fastest time constant of the closed interval distribution; Colquhoun, 1988), which means that longer closed durations were considered as interburst intervals. Interburst closed intervals of a lifetime between ~3 and 10 ms (double asterisks) could be distinguished from intervals lasting several

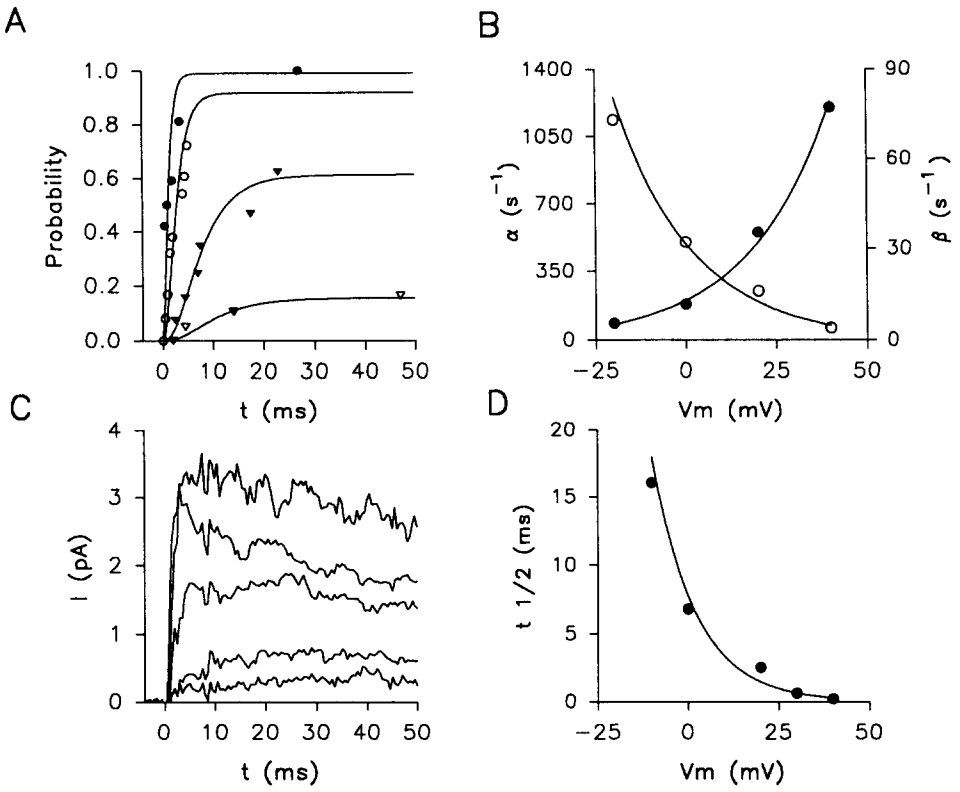

FIGURE 2. Voltage dependence of K_{O_2} channel activation. (*A*) Cumulative first latency histograms obtained at −20 (▽), 0 (▼), +20 (○), and +40 (●) mV in an inside-out patch. Correction for the number of channels in the patch ($N = 2$) was performed as indicated in Methods. Solid lines drawn over the data points are the fitted functions following the model of Scheme 2 scaled to the number of blanks at each membrane potential. (*B*) Estimated values of α (*filled circles*) and β (*open circles*) obtained from fittings to first latency at various membrane potentials. The solid lines are the solutions of Eqs. 1 and 2 in the text. (*C*) Ensemble average currents obtained in an outside-out patch with at least three K_{O_2} channels in response to pulses from −80 to −20, −10, 0, +20, and +40 mV (from bottom to top). (*D*) Half-time to peak ($t_{1/2}$) from averages in *C* vs. membrane voltage. Data are fitted to an exponential function with a slope factor of −12 mV. Effective cutoff frequency = 0.95 kHz and sampling interval = 250 μs. Solutions: standard Na, TTX//130 K, 10 EGTA.

tens to hundreds of milliseconds (triple asterisks) or even longer (see also Fig. 5*A*). The intraburst closed events and the short-lasting interburst intervals have durations smaller than the first latency and are, in principle, compatible with transitions between the open and closed states of the activation pathway. However, the duration

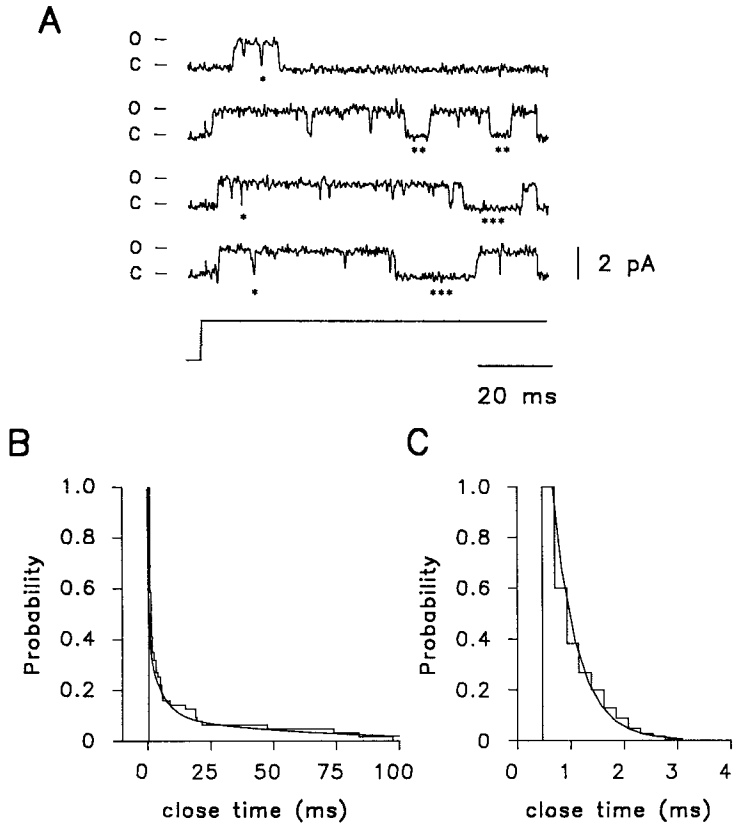

FIGURE 3. Closed interval distribution. (*A*) Representative single-channel recordings from an inside-out patch with $N = 1$ K_{O_2} channel during depolarizations from −80 to +20 mV. Examples of intraburst (*) and short- (**) and long- (***) lasting interburst intervals are illustrated. (*B*) Cumulative histogram of closed intervals during 400-ms pulses to +20 mV. A distribution function with three exponential components is superimposed on the data. The estimated time constants and weighting factors are: $\tau_1 = 506$ μs ($a_1 = 0.61$), $\tau_2 = 5.4$ ms ($a_2 = 0.1$), and $\tau_3 = 58.4$ ms ($a_3 = 0.28$). Number of events = 164. (*C*) Cumulative distribution of closed events shorter than or equal to 3 ms. A single exponential function with $\tau = 0.46$ ms is superimposed on the histogram. Number of events = 82. In the cumulative distributions presented in this and following figures the fitted function specifies the probability that an interval duration was longer than the time on the abscissa. Sampling interval = 250 μs and imposed time resolution = 468 μs. Solutions: standard Na, TTX//130 K, 10 EGTA.

of the long-lasting interburst intervals is clearly longer than any of the first latency values observed at this membrane potential; hence, it can be assumed that they represent transitions to a reversible inactivated state (Iverson and Rudy, 1990; Zagotta and Aldrich, 1990).

As indicated in Methods, a precise quantitative analysis of closed intervals was hampered by the difficulty in obtaining patches with one channel and by the fact that

Published September 1, 1992

at −80 mV K_{O_2} channels require a resting period of at least 30–40 s to recover completely from inactivation, which prevents rapid pulsing. Due to these limitations the parameters estimated must be taken only as approximate although they have the value that they come from measurements done in patches (n = 3) containing one K_{O_2} channel where we could compare in each case the distributions at normal and low P_{O_2}. Under normoxic conditions, closed interval distributions were consistently best fitted by a three-exponential function with average time constants of 0.5, 4.3, and 180 ms at +20 mV (Fig. 3 *B* and Table I). The weight of each component of the distribution was also consistent in the three patches studied. These data further

TABLE I

Kinetic Parameters of K_{O_2} Channels in Control and Hypoxic Solutions

	Control	Hypoxia
Median first latency (ms) (6)	2.15 ± 1.31	4.18 ± 1.42*
Closed time distribution (3)		
τ1 (ms)	0.5 ± 0.13	0.47 ± 0.13
Amplitude	0.68 ± 0.16	0.77 ± 0.1
τ2 (ms)	4.32 ± 2.7	3.84 ± 2.4
Amplitude	0.17 ± 0.1	0.13 ± 0.02
τ3 (ms)	180 ± 194	217 ± 289
Amplitude	0.15 ± 0.1	0.1 ± 0.09
Open time distribution		
τ_o (ms) (3)	35.4 ± 21	34 ± 18
τ'_o (ms) (1)	8.93	8.98
Burst length distribution (3)		
τ_b (ms)	46.5 ± 6	47.6 ± 10.7
Number of bursts per trace distribution (p) (3)	0.41 ± 0.07	0.55 ± 0.06**
Probability of blanks (5)	0.18 ± 0.02	0.47 ± 0.08*

Values are given by mean ± SD and the number of patches is given in parentheses. τ'_o values are from an experiment after correction for unresolved events. In the number of bursts per trace distribution, p is the probability for the transition from state I_0 to I_1 (see Scheme 4). All measurements were done during pulses to +20 mV.

*Statistically significant difference with respect to control values (paired t test, $\alpha < 0.01$).

**Significance level $\alpha = 0.116$ (see text for further details).

suggest that there are at least three kinetically different closed states from which K_{O_2} channels can reopen.

The fast intraburst closed intervals can be explained by adding to Scheme 2 a short-lived closed state (C_4) from where channels can flicker to the open conformation. In agreement with this idea, the distribution of the closed events <3 ms, shown expanded in Fig. 3 *C*, was best fitted by an exponential function with a time constant of 0.46 ms. Intraburst open time distributions were fitted too by a single exponential function that after correction for missed events yielded a mean open time value of 8.9 ms at +20 mV (see below). The three possible kinetic diagrams compatible with the

fast O/C_4 transitions are shown in Scheme 3 (*a–c*):

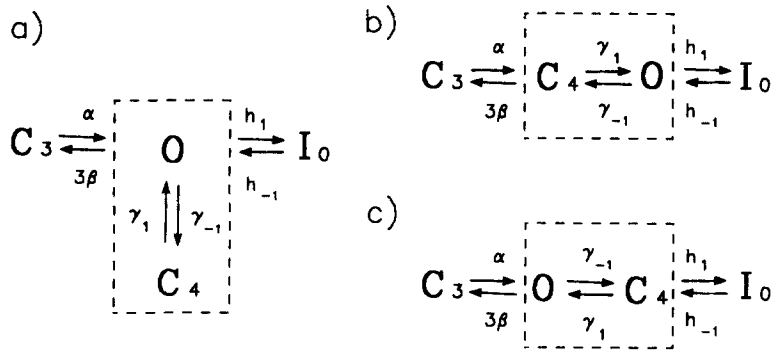

SCHEME 3

In these diagrams transitions between states O and C_4 (included within a box) configurate a burst which can terminate by the channel entering either states C_3 or I_0. Fits to first latency distribution cannot clearly distinguish among the various alternatives because the transition from C_4 to O is fast and its contribution to the first latency is negligible. Nevertheless, the analysis of burst durations suggests that the possibilities represented in *a* or *c* are preferable to *b* (see Fig. 4 *C*). Interestingly, the values estimated at +20 mV for the rate constants that characterize O/C_4 transitions (γ_1 = 2,200 s^{-1} and γ_{-1} = 110 s^{-1}) are quite comparable to those of *Drosophila* A-type (Solc and Aldrich, 1990; Zagotta and Aldrich, 1990) and squid (Perozo et al., 1991) K^+ channels that, in other aspects, are kinetically different from the K_{O_2} channels.

Open intervals and burst duration distributions. The distribution of sojourns in the open state, measured in patches with one or at most two observable channels, were fitted by a single exponential functions (Fig. 4 *A*). Adding more exponential terms did not result in significantly better fits. These results reveal that K_{O_2} channels have a single open state. At +20 mV the estimated mean open time was 34.5 ms (n = 5; see Table I), although this value is surely an overestimation because, as indicated above, many fast transitions to the intraburst closed state (C_4 in Scheme 3) may have been missed. We found that the dwell open time increases with depolarization but did not attempt to study this parameter in detail. Alternatively, we studied the voltage dependence of burst duration, a parameter that can be measured without the restrictions imposed by the time resolution. Burst duration distributions were also fitted by single exponential functions (Fig. 4 *B*) and at +20 mV the estimated mean value was 46.5 ms (n = 3, Table I). It was found, however, that burst length increases with membrane depolarization (Fig. 4 *C*). Because O/C_4 transitions are fast and these states reach equilibrium rapidly, the voltage dependence of the mean burst duration (τ_b) could be explained by the relations:

$$\tau_{b(V)} = 1/[(3\beta_{(V)} + h_1)\cdot p_o] \quad (3)$$

$$\tau_{b(V)} = 1/[p_c\cdot 3\beta_{(V)} + p_o\cdot h_1] \quad (4)$$

$$\tau_{b(V)} = 1/[p_o\cdot 3\beta_{(V)} + p_c\cdot h_1] \quad (5)$$

Published September 1, 1992

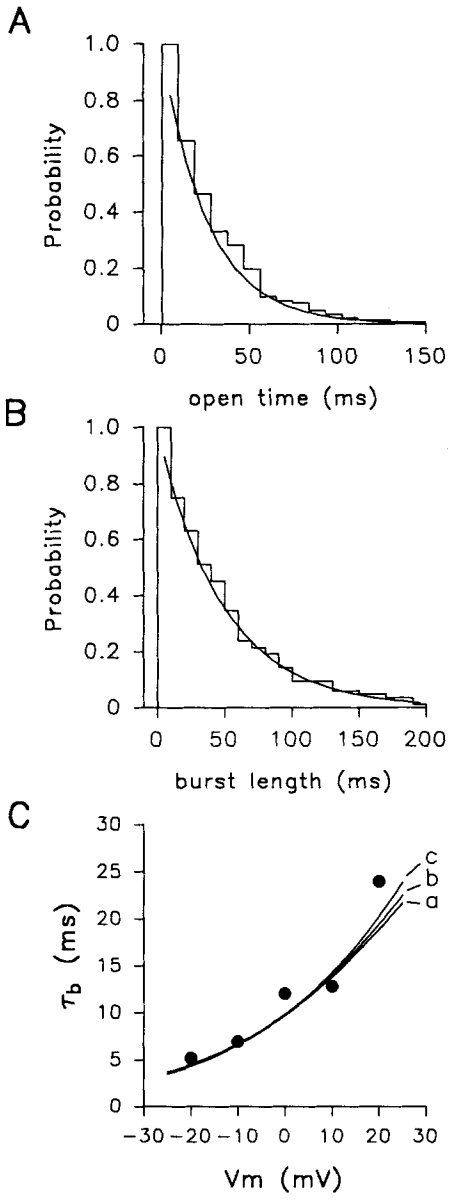

FIGURE 4. Open-time and burst duration distributions. Cumulative open-time (*A*) and burst duration (*B*) distributions at +20 mV. Single exponential fits are superimposed on the histograms. Time constants are 26.1 ms (*A*) and 48.5 ms (*B*). Data are from an inside-out patch with $N = 1$ K_{O_2} channel and in both cases 400-ms pulses were applied from −80 mV. Sampling interval = 250 μs and time resolution = 468 μs. Number of events = 142 and 84 for *A* and *B*, respectively. (*C*) Average burst duration (*ordinate*) calculated from 8–74 single events is plotted as a function of the membrane potential. The lines superimposed on the data points are fittings of Eqs. 3–5 (*a*, *b*, and *c*, respectively). The parameters obtained from the fittings were: $A_{3\beta} = 83.3$, 1,809, and 96.4 s^{-1}; $V_\beta = 21.6$, 22.1, and 24 mV; $h_1 = 20$, 18, and 200 s^{-1} for Eqs. 3–5, respectively. Data were obtained from an inside-out patch with $N = 2$ K_{O_2} channels. Imposed time resolution = 468 ms and sampling interval = 500 ms. Solutions: standard Na, TTX//130 K, 10 EGTA.

which apply, respectively, to diagrams *a*, *b*, and *c* in Scheme 3. In these equations 3β and h_1 are the rate constants determining the exit of the channels from flickering between states O and C_4. Since h_1 is presumed to be unaltered by voltage, the change of τ_b as a function of the membrane potential comes from the voltage dependence of 3β. On exiting from the flickering configuration, the fate of the channels depends on the probability of residence in states O (p_o) and C_4 (p_c) during a burst. These

probabilities are given by:

$$p_o = \gamma_1/(\gamma_1 + \gamma_{-1}) \quad (6)$$

$$p_c = \gamma_{-1}/(\gamma_1 + \gamma_{-1}) \quad (7)$$

Solutions to Eqs. 3–5, shown superimposed on the data points in Fig. 4, all fitted almost equally well the experimental observations in the membrane potential range studied, but we found diagram *c* preferable because it yielded the most appropriate estimates of 3β and h_1 (42 and 200 s^{-1}, respectively, at +20 mV) for the reconstruction of the macroscopic O_2-sensitive K^+ current (see Fig. 13).

Number of inactivated states and inactivation time course. Fig. 5 *A* illustrates the activity of K_{O_2} channels during 3-s depolarizing pulses to +20 mV. The channels open and close several times during the pulse and although most of the events appear grouped in the initial 500 ms, reopenings can be observed after closed periods lasting up to several hundred milliseconds or even more than 1 s (asterisks). However, during sufficiently long voltage steps, or stationary depolarizations, the activity of K_{O_2} channels ceases completely. This suggests the existence of another inactivated state that is absorbing and thus nonreversible at depolarized membrane potentials. The ensemble average of Fig. 5 *B* shows that most of the channels are inactivated after ~1 s and that the time course of K_{O_2} channel inactivation can be matched by a double exponential function, superimposed on the current average, with time constant values at +20 mV of ~25 and 281 ms. Like ensemble averages of K_{O_2} channels, the decay of the macroscopic O_2-sensitive K^+ current follows a double exponential time course, with fast and slow time constants on the order of tens and hundreds of milliseconds, respectively (Fig. 5 *C*). The scaled current traces at 0 and +20 mV, superimposed in Fig. 5 *D*, indicate that at positive membrane potentials the fast component is speeded up slightly but the slow component remains almost unaltered. This is probably a result of the voltage dependence of the first latency; at 0 mV completion of channel opening is slower and more scattered than at +20 mV (see Fig. 2 *A*), and hence a coupled model of inactivation would predict that those channels that open with longer latency will also begin to inactivate later on during the pulse.

If inactivation is strictly coupled to activation, channels must open before they inactivate. It is known, however, that voltage-dependent channels can occasionally inactivate without opening (Bean, 1981; Horn et al., 1981). Transition from closed to inactivated states is the most likely explanation for the occurrence of blank records in K_{O_2} and other K^+ channels (Hoshi and Aldrich, 1988; Cooper and Shrier, 1989; Zagotta and Aldrich, 1990). Blank records could also appear due to cumulative inactivation or because channels open with a latency longer than the pulse duration. In our experimental conditions these two possibilities could be discarded because blank records were observed at fairly positive voltages (at +20 or +40 mV) and during depolarizing pulses lasting > 1 s applied with an interval of 45 s (a time period at which removal from inactivation is complete). Fig. 6 shows that the probability of obtaining blank records is drastically influenced by the membrane potential; a high probability (0.7) is observed at −40 mV but it drops to ~0.2 at +20 mV.

Minimal kinetic model of K_{O_2} channel gating. The data presented so far are compatible with the model shown in Scheme 4, which includes the minimum number

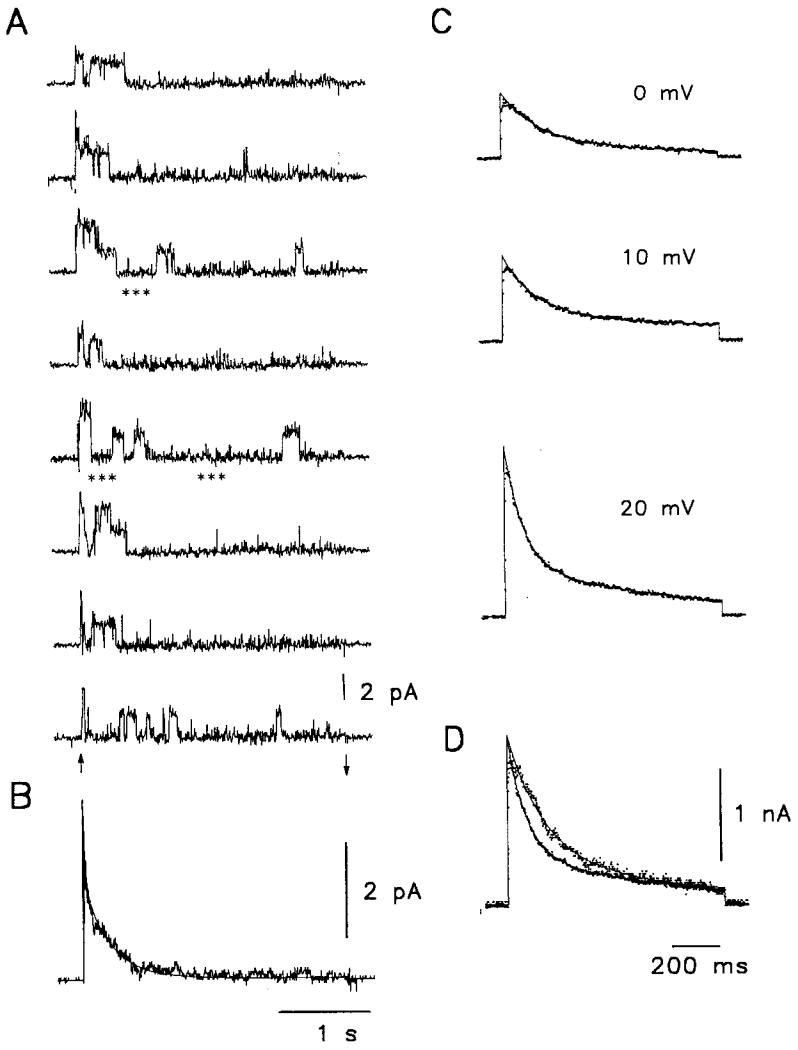

FIGURE 5. Inactivation of K_{O_2} channels and the O_2-sensitive K^+ current. (*A*) Representative recordings from an outside-out patch with at least three channels during 3-s pulses to +20 mV. Some examples of long-lasting interburst intervals are indicated by triple asterisks. Effective cutoff frequency = 0.95 kHz and sampling interval = 3.9 ms. (*B*) Ensemble average current from 26 depolarizations delivered every 60 s. A function with two exponential terms and a constant (c) was fitted to the decay phase of the current (the first 5 ms from the onset of the pulse are not included), giving estimates of c = 0.02 pA, τ_1 = 24.9 ms (a_1 = 2.1 pA), and τ_2 = 280.9 ms (a_2 = 2.5 pA). Solutions: standard Na, TTX//standard K, 10 EGTA. (*C*) Whole-cell currents generated by pulses from −80 mV to the indicated membrane potentials. A double-exponential function is fitted to the decay phase of the current discarding the first 5 ms of the pulse. Estimated parameters are: at 0 mV, τ_1 = 163.4 ms (a_1 = 0.53 nA) and τ_2 = 900.9 ms (a_2 = 0.18 nA); at +10 mV, τ_1 = 128.5 ms (a_1 = 0.58 nA) and τ_2 = 787.7 ms (a_2 = 0.26 nA); at +20 mV, τ_1 = 78.1 ms (a_1 = 1.27 nA) and τ_2 = 714.2 ms (a_2 = 0.57 nA). (*D*) Scaled currents and fittings obtained at 0 and +20 mV. Effective cutoff frequency = 10 kHz; sampling interval = 2 ms. Solutions: standard Na, TTX//standard K, 10 EGTA.

of states and transitions necessary to account for the major gating features of K_{O_2} channels. A summary of the kinetic parameters obtained from the theoretical fits to the single-channel data is given in Table I (control), and Fig. 13 shows that this model can adequately reproduce the time course of the macroscopic O_2-sensitive K^+ current.

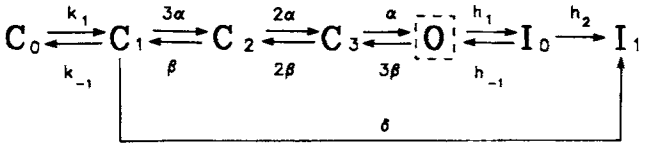

SCHEME 4

Qualitatively this sequential scheme works as follows. At negative holding potentials the rate constant α is much smaller than β and therefore most channels are

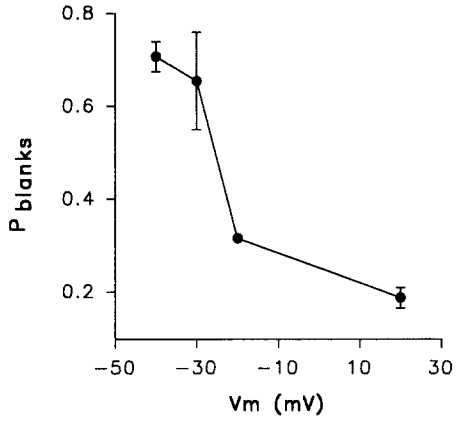

FIGURE 6. Voltage dependence of the probability of observing a blank record. The fraction of records that elicited no openings during 200- or 400-ms pulses (*ordinate*) is plotted against the step potential (*abscissa*). Values are mean ± SD from five experiments. Correction for the number of channels in the patch was done in two of the five experiments where two K_{O_2} channels were present in the patch. Pulses were delivered from a holding potential of −80 mV separated by an interval of at least 45 s.

distributed between states C_0 and C_1. The rate constants k_1 and k_{-1} are assumed to be regulated by P_{O_2} and under normoxic conditions the equilibrium C_0/C_1 is displaced toward C_1 (see below). Upon depolarization the opposite change of α and β shifts the equilibrium toward the open state. This state is relatively unstable and channels flicker between the open and a short-living closed conformation, which configurates a burst. In fitting the data we found it preferable to place state C_4 after the open state (see Scheme 3), but since this is not necessarily the only kinetic possibility, states O and C_4 are lumped together in Scheme 4 and the burst configuration is represented by the box enclosing the open state. Bursts can terminate by the channels either returning to state C_3 or entering the reversible inactivated state (I_0). The former possibility is infrequent at positive membrane potentials as 3β becomes smaller with depolarization. During maintained depolarizations channels can make several bursts but they enter progressively into an absorbing inactivated state (I_1), and eventually their activity ceases completely.

Scheme 4 also includes closed-state inactivation, which is a quite apparent feature of K_{O_2} channels. Although we have no direct evidence, closed to inactivated transitions are assumed to begin at state C_1. This is the preferable way to explain the effect of low P_{O_2} on channel gating (see below). It is also presumed that the closed-state inactivation rate constant (δ) is voltage independent, as is the inactivation rate constant in the normal sequence (h_1); thus the apparent voltage dependence of the appearance of blank records is probably a result of the voltage dependence of the activation rate constant (α). Our data also suggest that in most closed to inactivated transitions the channels end at the absorbing state (I_1). Transitions to the reversible inactivated state (I_0) would predict the appearance at positive voltages of openings with an unusually long latency (over 100 or 200 ms) which were never observed in our experiments.

TABLE II

Deactivation Kinetics of Macroscopic K^+ Currents

	Control	Hypoxia
Fast component		
Time constant	3.12 ± 0.75	3.63 ± 0.32
Amplitude	1.37 ± 0.47	0.66 ± 0.15
Slow component		
Time constant	40.52 ± 28.44	39.87 ± 26.24
Amplitude	0.96 ± 0.23	0.58 ± 0.06

Time constant values are given in milliseconds and amplitudes in nanoamperes by the mean ± SD (n = 2 patches). Data were obtained by double-exponential fit to tail currents recorded at the instant of repolarization to −80 mV from a membrane potential of +20 mV in cells bathed in an external solution with 130 mM KCl. Differences between time constants estimated in control and hypoxic solutions are not statistically significant (t test, $\alpha > 0.05$)

Kinetic Modifications Induced by Lowering P_{O_2}

Based on the kinetic scheme of K_{O_2} channel gating presented in the previous section, in what follows we focus on a systematic analysis of the modifications induced by hypoxia. All the data presented were obtained from channels exposed to both normoxic and hypoxic solutions and, thus, to facilitate comparison, the average values of the parameters obtained from fittings of the data in the two experimental conditions are shown in Tables I, II, and III.

Low P_{O_2} retards channel activation. Fig. 7 *A* shows a family of macroscopic K^+ currents from a glomus cell at the indicated membrane potentials. Current traces recorded in a low P_{O_2} solution (H: P_{O_2} = 5–10 mmHg) can be compared with those obtained at normal P_{O_2} (C: P_{O_2} = 150 mmHg). Recovery from hypoxia is almost perfect and an example is shown at +40 mV (trace R). As reported previously (López-López et al., 1989), low P_{O_2} produces an attenuation of the K^+ current amplitude that is more pronounced on moderate depolarization; a voltage dependence similar to the decrease of K_{O_2} channel open probability during exposure to hypoxia has been described (Ganfornina and López-Barneo, 1992). In parallel to this

TABLE III

Inactivation Time Course of K_{O_2} Channels

	Control	Hypoxia
Fast component		
τ (ms)	32.6 ± 13	47.4 ± 12
Amplitude (normalized)	0.47 ± 0.01	0.9 ± 0.05*
Slow component		
τ (ms)	267 ± 39	351 ± 139
Amplitude (normalized)	0.52 ± 0.01	0.09 ± 0.05*

Values are given by the mean ± SD (n = 3 patches). Data were obtained by double-exponential fit to ensemble averages. Pulse duration = 3 s. Membrane potential = +20 mV. *Statistically significant differences with respect to the control values.

effect, low P_{O_2} slows down the activation time course of the K^+ current, as illustrated by the scaled traces in Fig. 7 *B*. Activation kinetics of the O_2-sensitive K^+ current are quantified in Fig. 8 *A* by the time to reach half-maximal current amplitude ($t_{1/2}$) in control and under hypoxic conditions at various membrane potentials. At +20 mV, for example, low P_{O_2} reduces by almost 50% the speed of activation. These effects of hypoxia were very reproducible and qualitatively similar in the 79 type I cells tested so far.

The results of Fig. 7 predict, on the basis of a sequential model of gating, that low P_{O_2} would retard K_{O_2} channel first opening, as is in fact shown in Fig. 8 *B*, where cumulative first latency distributions at +20 mV obtained in normoxic and hypoxic solutions are compared. The average median first latency values calculated in six patches are given in Table I. In good agreement with the effect on the macroscopic current, at +20 mV hypoxia increases by almost a factor of two the median first latency of K_{O_2} channels. The increase of first latency induced by low P_{O_2} could be due to stabilization of any, or several, of the closed states existing in the activation

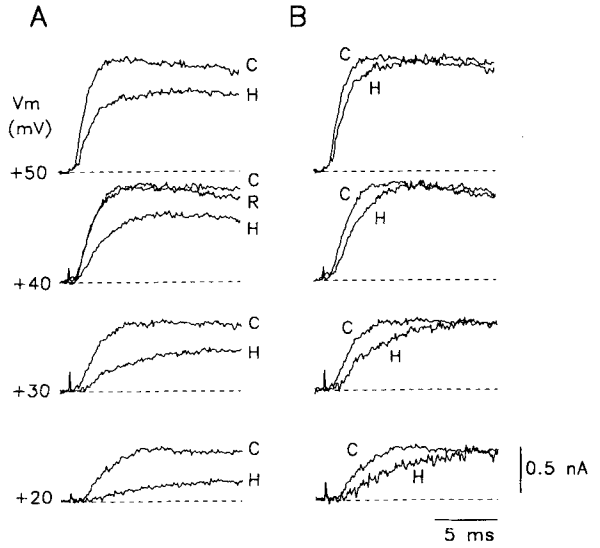

FIGURE 7. Effect of low P_{O_2} on the rising phase of the macroscopic O_2-sensitive K^+ current. (*A*) Current generated upon step depolarizations from −80 mV to the indicated membrane potentials in control (*C*: P_{O_2} = 150 mmHg) and hypoxic (*H*: P_{O_2} ~ 5–10 mmHg) solutions. Recovery (*R*) after returning to control solution is shown at +40 mV. (*B*) The same traces as in *A* are shown scaled to compare their time course. Effective cutoff frequency = 10 kHz and sampling interval = 100 μs. Solutions: 80 K, TTX//standard K, 10 EGTA.

pathway. The simpler explanation is that hypoxia specifically influences the transition between states C_0 and C_1. The solid lines in Fig. 8 *B* are the theoretical fits to first latency histograms obtained from a patch exposed to normoxic and hypoxic solutions following the kinetic diagram of Scheme 2. In this and in two more patches good fittings were obtained in the two experimental conditions without altering the values of α and β and assuming that the modifications in the rate constants k_1 and k_{-1} upon exposure to extreme hypoxia ($P_{O_2} \approx$ 5–10 mmHg) determine that the percentage of channels in state C_0 changes from 2.5 to 73.3% (see Fig. 13). Thus, at −80 mV (a potential at which most of the channels are in state C_1) hypoxia shifts the equilibrium further to the left and favors the residence of the channels in the closed

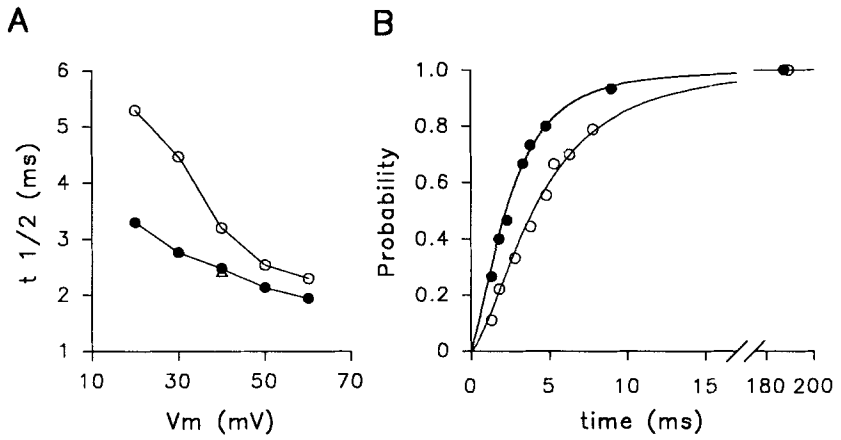

FIGURE 8. Effect of hypoxia on the activation time course of the macroscopic O_2-sensitive K^+ current and K_{O_2} channels. (*A*) Half-time to peak of the macroscopic K^+ current ($t_{1/2}$, *ordinate*) plotted vs. step voltage (V_m, *abscissa*) in control (*filled circles*) and hypoxic (*open circles*) conditions. Data were obtained from the experiment shown in Fig. 7. The open triangle indicates the recovery after returning to the control solution. (*B*) Cumulative first latency distributions obtained in an inside-out patch with N = 1 K_{O_2} channel in control (*filled circles*, P_{O_2} = 150 mmHg) and hypoxic (*open circles*, $P_{O_2} \sim$ 5–10 mmHg) conditions. Pulses from −80 to +20 mV were delivered every 30 s while alternating exposure to control and hypoxic solutions was applied. Data are fitted by the model of Scheme 2 using the rate constant values indicated in Fig. 13 *A*. Effective cutoff frequency = 0.95 kHz; sampling interval = 250 μs. Solutions: standard Na, TTX//130 K, 10 EGTA.

state C_0. This could explain why low P_{O_2} increases the activation latency without affecting α and its more pronounced effect at moderate depolarizations, since it can be expected that the relative change of k_1 and k_{-1} will have a larger influence on activation at potentials at which α is not too large.

Transitions near the open state are unaffected by hypoxia. It was shown before that after the first opening K_{O_2} channels undergo reversible transitions to adjacent nonconducting states (Schemes 3 and 4). Fig. 9 *A* shows the cumulative closed interval histogram obtained from a channel exposed to hypoxia and superimposed (solid line) a three-exponential distribution function obtained by fitting the experimental values. The fit obtained in the same patch with normal P_{O_2} and at the same

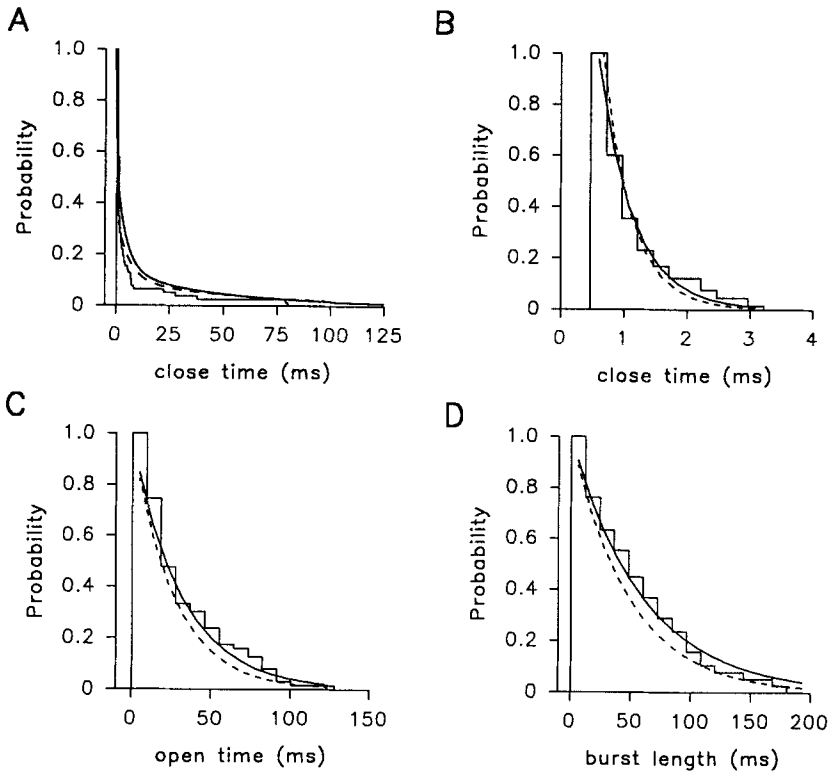

FIGURE 9. Closed-time, open-time, and burst length distributions at low P_{O_2}. (*A*) Cumulative histogram of closed-time intervals from records of the same experiment shown in Fig. 3 obtained while the patch was bathed in a hypoxic solution (P_{O_2} ~ 5–10 mmHg). The continuous line is the distribution function fitted to the data (τ_1 = 0.44 ms, a_1 = 0.81; τ_2 = 4.3 ms, a_2 = 0.14; τ_3 = 46 ms, a_3 = 0.05; number of events = 81). The fitting obtained under normoxic conditions is also shown (*dashed line*) for comparison (see Fig. 3 *B*). These distributions were not statistically different (U test, $\alpha > 0.05$). (*B*) Cumulative histogram of closed events $\leq$3 ms (see Fig. 3 *C*). The single exponential functions obtained in hypoxic (continuous line, τ = 0.55 ms) and control (dashed line, τ = 0.46 ms) conditions are superimposed on the histogram. Number of events = 66. Data were obtained from an inside-out patch with N = 1 K_{O_2} channel. Sampling interval = 250 μs; imposed time resolution = 468 μs. Solutions: standard Na, TTX//130 K, 10 EGTA. (*C* and *D*) Open-time (*C*) and burst length (*D*) cumulative distributions in hypoxia during 400-ms pulses from −80 to +20 mV. Number of events = 61 and 38, respectively. The scaled single-exponential distribution functions are shown superimposed to the histograms. The fittings obtained under normoxic conditions (*dashed lines*) are also shown for comparison. Data were obtained from an inside-out patch with N = 1 K_{O_2} channel. Sampling interval = 250 μs; imposed time resolution = 468 μs. Solutions: standard Na, TTX//130 K, 10 EGTA.

membrane potential (+20 mV; see Fig. 3 *B*) is also shown (discontinuous line). Average values of the estimated parameters (time constant and relative amplitude of each component) obtained from the fits to closed interval distributions from several patches (Table I) indicate that they are not significantly modified by low P_{O_2} (paired

Published September 1, 1992

t test). In agreement with these results, the cumulative histogram of intraburst closed intervals measured during exposure to low P_{O_2}, plotted separately in Fig. 9 *B*, is fitted by a single exponential function (solid line; $\tau = 0.51$ ms) that does not appreciably differ from the one estimated under normoxic conditions (discontinuous line, $\tau = 0.46$ ms; see also Fig. 3 *C*). Thus, it can be concluded that the rate constants that determine the exit of the channels from the reversible nonconducting states (either a closed state or the reversible inactivated state) are unaffected by hypoxia.

Fig. 9 also illustrates the open time (C) and burst duration (D) distributions of K_{O_2} channels in low P_{O_2}. In both cases the solid lines are the single exponential functions that fitted the data and, to facilitate comparison, the discontinuous lines are the functions obtained at normal P_{O_2}. Average values of the mean open time (τ_o) at +20 mV from five patches studied in the two experimental conditions are given in Table I, which also includes estimates from an experiment after correction for missed events (τ'_o) as indicated by Colquhoun (1988). Since no statistically significant difference was found (U test) between the distributions obtained in the two experimental conditions, it should be concluded that low P_{O_2} does not alter the mean open time of K_{O_2} channels. Further support for this idea is provided by the fact that the burst length distribution, a variable that can be measured without the restriction imposed by the time resolution, has a similar single exponential shape in control and under hypoxic conditions (Fig. 9 *D*; Table I). These distributions were not significantly different (U test), indicating that the rate constants h_1 and 3β, which determine burst length (i.e., the exit of the channels from flickering between states C_4 and O; see Scheme 3), are not modified by low P_{O_2}.

The experiments described in the previous paragraphs show that at +20 mV transitions between the open state and any of the adjacent states are not under the influence of O_2 tension. We also tested whether at negative potentials closing of K_{O_2} channels is similar in control and hypoxic conditions. These experiments were performed by recording macroscopic K^+ tail currents in cells bathed in high K^+ solutions. Channels were opened by 20-ms step depolarizations to +20 mV and at the instant of repolarization to −80 mV (indicated by the arrows in Fig. 10) we recorded tail currents whose time course reflect the kinetics of the transition to nonconducting states of the channels open at the end of the pulse. At −80 mV, the tails probably represent deactivation of the channels (returning to closed states in the activation pathway), although they may also have a small component due to channel inactivation. In all cells studied ($n = 4$) tail currents were fitted by the sum of two exponential components, drawn superimposed on the current traces in the example of Fig. 10, *A* and *B*. Low P_{O_2} produced a perfectly reversible attenuation in the amplitude of the two components of the tails, reflecting the decrease in the number of channels open during the pulse, but their respective time constant values were unchanged (Table II).

Low P_{O_2} favors closed-state inactivation. Besides the lengthening of the activation latency, one of the most striking effects of hypoxia is a marked increase in the appearance of blank records. The average values of blank record probability at +20 mV in five patches exposed to normoxic and low P_{O_2} solutions are given in Table I. Hypoxia increased blank probability by a factor of almost 2.5, a relative change comparable to that induced by low P_{O_2} on the activation kinetics of the macroscopic

O_2-sensitive K^+ current and the median first latency of K_{O_2} channels at the same membrane potential. These results suggest that low P_{O_2} highly favors the direct transition of K_{O_2} channels from closed to inactivated states. Since in our model closed to inactivated transitions occur from state C_1 and the voltage-dependent forward rate constant in the activation pathway (α) is not affected by hypoxia, the higher occurrence of blank traces leads us to suggest that low P_{O_2} increases the rate constant δ, perhaps due to a further stabilization of state I_1 or to a decrease in the activation energy of the transitions leading to the absorbing inactivated state.

Low P_{O_2} favors the transitions to the absorbing inactivated state. The effect of low P_{O_2} on the inactivation time course of K_{O_2} channels is illustrated in Fig. 11 by ensemble average currents obtained from an outside-out patch containing two channels activated by 3-s pulses to +20 mV. The control record (the darker trace in Fig. 11 *A*) shows that in ~0.5–1 s K_{O_2} channels inactivate almost completely (see also Fig. 5, *A*

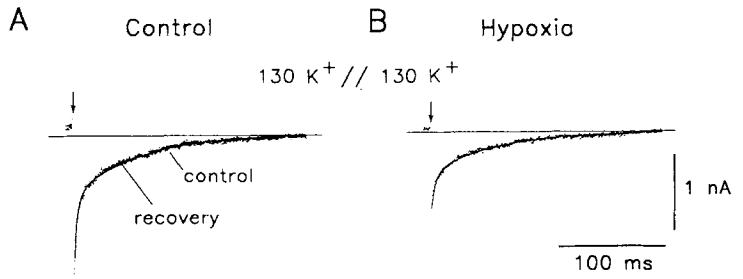

FIGURE 10. Effects of hypoxia on the deactivation kinetics of the O_2-sensitive K^+ current. Tail currents elicited upon repolarization to −80 mV after a 20-ms pulse to +20 mV with a P_{O_2} of 150 mmHg (*A*, control and recovery) and a P_{O_2} < 5 mmHg (*B*). The instant of repolarization is indicated by the arrows. Note the smaller amplitude of the current at the end of the pulse in hypoxia compared with control. Tail currents are fitted by a double-exponential function whose estimated parameters are shown in Table II. The first two sample points of the tails were not included in the fitting. Effective cutoff frequency = 10 kHz; sampling interval = 500 μs. Solutions: 130 K, EGTA//130 K, 10 EGTA.

and *B*). Exposure to hypoxia produces a decrease in the peak amplitude of the average current and accelerates inactivation, which in this condition is nearly complete in <500 ms (Fig. 11 *B*). This effect is reversible, as shown by the recovery trace (the lighter trace in Fig. 11 *A*), and was consistently observed in all patches studied (n = 29). In the two experimental conditions, the inactivation time course was fitted by the sum of two (fast and slow) exponential functions and the mean values of the time constants as well as the weight of each component estimated in several patches are given in Table III. Low P_{O_2} produces a drastic reduction of the slow component of inactivation, leaving a fast component with an almost unaltered time course. Since it was shown before that hypoxia does not modify the rate constants that characterize the transitions between the open and the reversible inactivated states (h_1 and h_{-1} in Scheme 4), we interpret these results as indicating that low P_{O_2} favors the transition from state I_0 to I_1. This interpretation also predicts

Published September 1, 1992

that low P_{O_2} should disfavor reopening of K_{O_2} channels from state I_0 and therefore decrease the number of bursts per trace. This discontinuous variable is expected to follow a geometric distribution (Colquhoun and Sigworth, 1983), with the unknown parameter (p) being the probability of entering the absorbing inactivated state I_1. The number of bursts per trace distribution was well fitted to a single geometric distribution function in three patches with one K_{O_2} channel. The estimated average values of p were 0.41 in control and 0.55 in hypoxic solutions (Table I). The difference between these two values, although varying in the direction of the predictions of the model, was not statistically significant ($\alpha = 0.116$). Nonetheless, it must be noticed that the number of bursts per trace and the difference of p in the two experimental conditions have surely been underestimated, since they were calculated from data obtained during pulses of 200 or 400 ms, a duration too short for allowing complete inactivation of the channels.

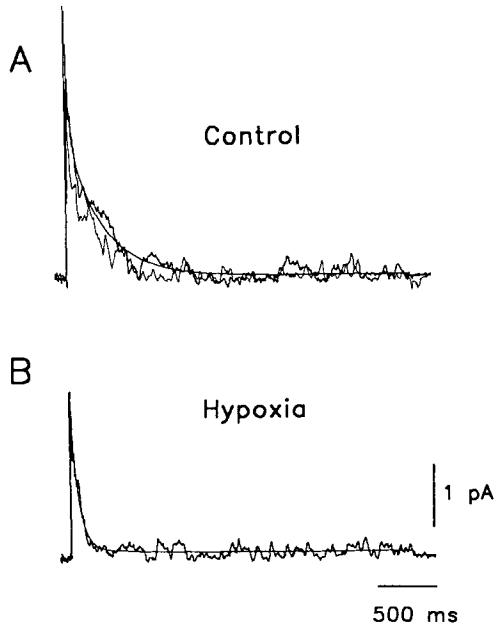

FIGURE 11. Modification of the inactivation time course of K_{O_2} channels by hypoxia. (*A*) Ensemble average of records obtained during 3-s pulses to +20 in an outside-out patch with N = 2 K_{O_2} channels exposed to a normoxic solution. The lighter trace shows the average obtained after recovery from a 4-min exposure to low P_{O_2}. (*B*) Ensemble average of single-channel records obtained during exposure to hypoxia. Smooth lines in *A* and *B* are the fittings to double-exponential functions whose estimated parameters are shown in Table III. Effective cutoff frequency = 1 kHz; sampling interval = 3.9 ms. Pulses were delivered with a minimum interval of 45 s. Solutions: standard Na, TTX//standard K, 10 EGTA.

The modifications induced by hypoxia on the inactivation time course of K_{O_2} channels are summarized in Fig. 12. The two panels at the right of the figure show representative single-channel currents from an inside-out patch with one K_{O_2} channel exposed to control (*B*) and hypoxic (*D*) solutions. The respective ensemble average currents are plotted in *A* and *C*, illustrating that the probability of channel opening decreases in low P_{O_2}. Superimposed on the ensemble averages we have plotted the convolutions of the open time and first latency distributions (continuous smooth lines) and of burst duration and first latency distributions (discontinuous smooth lines) estimated in the two experimental conditions. These theoretical functions predict the time course of ensemble averages of inactivating channels that either open once (continuous line) or make a single burst (discontinuous line) per pulse

(Aldrich et al., 1983; Kirsch and Brown, 1989). Fig. 12 *A* illustrates that the time course of K_{O_2} channel open probability clearly deviates from any of these predictions because they normally make several bursts during a pulse, which slows down their inactivation time course. The deviation from the theoretical functions is, however, markedly reduced by low P_{O_2}, indicating that under this experimental condition

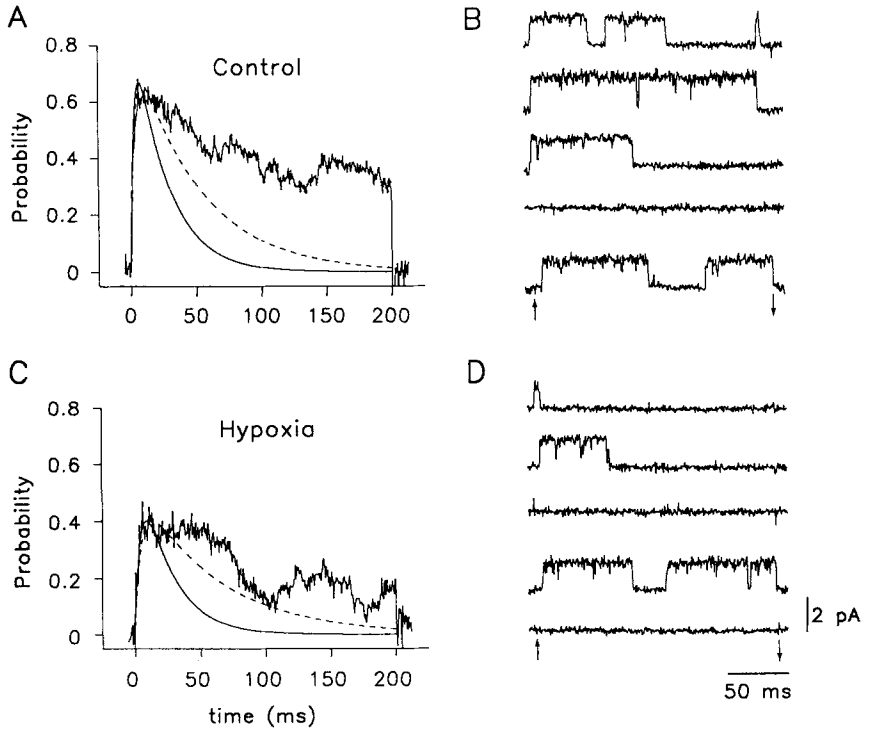

FIGURE 12. Effect of low P_{O_2} on K_{O_2} channel inactivation. (*B* and *D*) Representative recordings illustrating the activity of a K_{O_2} channel exposed to normoxic and hypoxic solutions, respectively. (*A* and *C*) Ensemble averages from a set of single-channel records obtained from the same inside-out patch (N = 1 K_{O_2} channel) exposed to control and hypoxic solutions. Ensemble averages are normalized by the single-channel amplitude. In both panels the continuous line is the convolution of the open-time and first latency distributions and the dashed line is the convolution of the burst length and first latency distributions calculated from the probability density functions estimated in the two experimental conditions. Effective cutoff frequency = 0.95 kHz and sampling interval = 500 μs. All measurements were done in traces obtained by 200-ms depolarizations to +20 mV delivered every 30 s. Solutions: standard Na, TTX//130 K, 10 EGTA.

reopening of K_{O_2} channels is less likely and, as a consequence, their inactivation time course follows more closely the predictions of a model with a single burst per trace (discontinuous line).

A model for the effect of hypoxia on K_{O_2} channel gating. Low P_{O_2} modifies specific transitions and states in K_{O_2} channels which can be simply summarized by assuming

that state C_0 is stabilized and transitions to state I_1 favored. The state diagram of K_{O_2} channel gating proposed in Scheme 4 is shown in Fig. 13 *A* with the values (in seconds^{-1}) estimated for the different rate constants at +20 mV under normoxic conditions (P_{O_2} = 150 mmHg). The values at low P_{O_2} (~5–10 mmHg) of the rate constants altered upon exposure to hypoxia are given in parentheses. As explained in the previous sections, the different variables were estimated from the fits to the

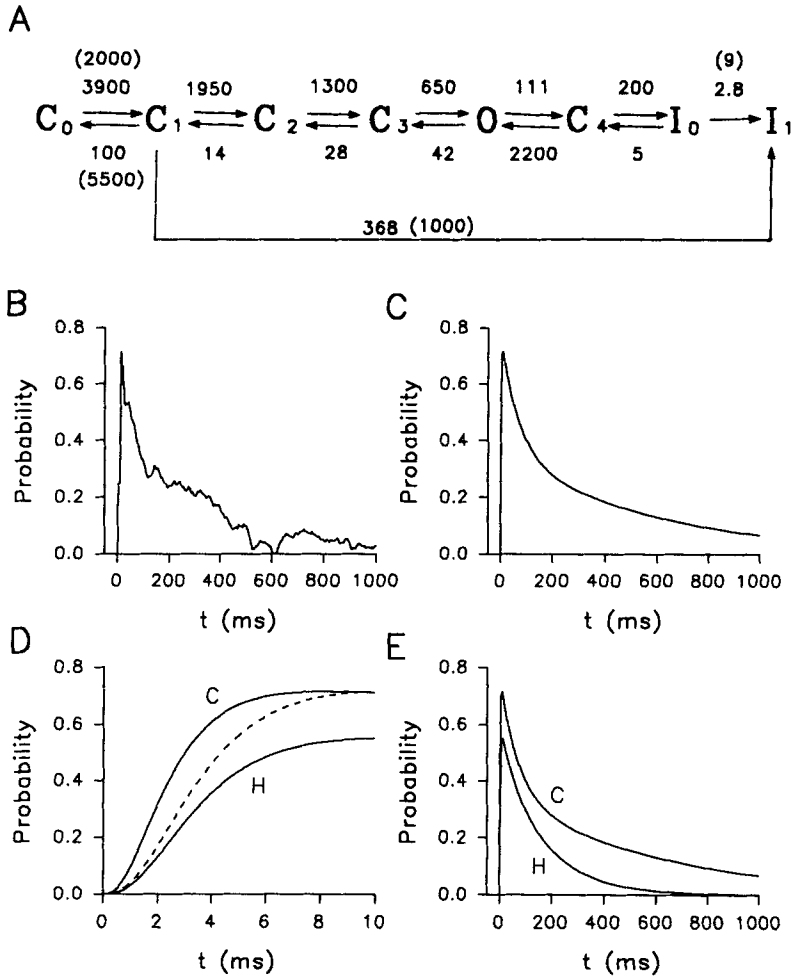

FIGURE 13. Kinetic model of K_{O_2} channel gating and modifications induced by low P_{O_2}. (*A*) State diagram of K_{O_2} channel gating (Scheme 4 in the text) with the numerical values of the rate constants at +20 mV in normoxic (P_{O_2} = 150 mmHg) and hypoxic (P_{O_2} ≈ 5 mmHg) conditions. In parentheses are the values of the rate constants altered upon exposure to low P_{O_2}. (*B* and *C*) Comparison of the time course of the ensemble average current of K_{O_2} channels (control record in Fig. 11 *A*) and the solution of the model under normoxic conditions and at +20 mV. (*D* and *E*) Predictions of the model under control (*C*) and hypoxic (*H*) conditions. In *D*, trace *H* has been scaled (*discontinuous line*) to the same amplitude as trace *C* to illustrate the deceleration of the activation time course at low P_{O_2}.

first latency and to the open and closed interval distributions. The rate constants h_2 and δ, specifying the irreversible transitions to the absorbing inactivated state, were calculated from:

$$pI_0\text{–}I_1 = h_2/(h_2 + h_{-1}) \quad (8)$$

and

$$p_b = \delta/(3\alpha + k_{-1} + \delta) \quad (9)$$

$pI_0 - I_1$ (Eq. 8) is the probability of entering the absorbing state estimated from fittings of the number of burst per trace distributions. This variable was increased by 15–25% to correct for the underestimation of the number of bursts since, as indicated above, it was calculated from pulses lasting less than the time required for complete inactivation of K_{O_2} channels.

We preferred to assume that closed-state inactivation begins at state C_1, rather than at state C_2 or C_3, because if this mode of inactivation occurs from a state near the open state, the increase of δ on exposure to low P_{O_2} produces by mass action an acceleration of the activation kinetics incompatible with the experimental findings. Given this assumption, the value of δ was estimated from Eq. 9, where p_b is the probability of blanks under normoxic conditions. At low P_{O_2}, we chose a value for δ such as to determine the same probability of blank traces as experimentally observed.

Our model quantitatively reproduces the activation and inactivation kinetics of the macroscopic O_2-sensitive K^+ current, as well as the peak open probability of K_{O_2} channels at various membrane potentials. In Fig. 13, *B* and *C*, we show, for comparison, the ensemble average current from a patch with one K_{O_2} channel at +20 mV (*B*) and the computer solution of the model at the same membrane potential (*C*). Adequate matching of the model to the experimental data can be further evaluated by its comparison with recordings of whole-cell K^+ currents (see, for example, the trace at +20 mV in Fig. 5 *C*). In Fig. 13, *D* and *E*, computer solutions of the model are shown under control (C) and low P_{O_2} (H) conditions, illustrating that its predictions (decrease in channel open probability, retardation of activation kinetics, and acceleration of inactivation time course) are in good agreement with the experimental results.

DISCUSSION

In this article we show that the major gating properties of K_{O_2} channels can be explained on the basis of a minimal kinetic scheme and that low P_{O_2}, rather than a general alteration of this scheme, reversibly modifies specific states and transitions. These findings explain the decrease in K_{O_2} channel open probability under exposure to low P_{O_2} and help to understand the role of K_{O_2} channels in regulating the excitability of glomus cells under normoxic and hypoxic conditions.

Kinetic Properties of K_{O_2} Channels

The kinetic model proposed for K_{O_2} channel gating is based on sequential schemes of other channels (see, for example, Armstrong and Bezanilla, 1977) and resembles in several ways the model developed by Zagotta and Aldrich (1990) for *Shaker* K^+

Published September 1, 1992

channels of *Drosophila* myotubes, albeit there are some qualitative and quantitative differences. The major features of the gating scheme are as follows: (*a*) Resting channels must traverse several closed states before opening. (*b*) K_{O_2} channels exhibit a single open state from which they flicker to a short-lived closed state. These fast transitions configurate a burst whose duration increases with membrane depolarization. (*c*) Termination of a burst occurs either by returning to a closed state in the activation pathway or by entering a reversible inactivated state. (*d*) During a maintained depolarization, channels normally make several bursts before they inactivate. Inactivation usually proceeds through the reversible inactivated state before entering an absorbing state. (*e*) Channels can directly inactivate, before opening, from a closed state of the activation pathway.

Fits to first latency histograms indicate that K_{O_2} channels traverse at least three closed states (C_1 to C_3) before opening. In our model, distribution of the channels between the left-most closed state (C_0) and state C_1 is assumed to be dependent on O_2 tension. Once open, K_{O_2} channels display several fast transitions to a nonconducting state of short lifetime. This indicates that, as in other K^+ channels (Magleby and Pallotta, 1983; Zagotta and Aldrich, 1990), the open state is relatively unstable and that in the process of ion conduction channels intermittently reside in a short-lived closed state (C_4 in Scheme 3).

In a number of voltage-gated K^+ channels (Zagotta and Aldrich, 1990; Perozo et al., 1991) it has been shown that the mean open time is independent of the membrane potential. However, it has also been reported that in some mammalian K^+ channels this parameter increases with depolarization (Hoshi and Aldrich, 1988; Cooper and Shrier, 1989), a result also observed in our analysis of K_{O_2} channel gating. If channels open intermittently, in the form of bursts, the open time is a variable whose estimation is, in many cases, subjected to a high degree of uncertainty, because many fast closed events are missed due to the limited recording bandwidth necessary to resolve single-channel currents. We preferred to study the voltage dependence of the burst duration, a parameter that can be measured with more accuracy, and found that in K_{O_2} channels it increases with depolarization. This is a distinct property that differentiates K^+ channels of glomus cells from native *Shaker* K^+ channels (Zagotta and Aldrich, 1990), and strongly suggests that after the first opening K_{O_2} channels can return to a closed state in the activation pathway. Thus, bursts terminate by channels entering either an inactivated state or a closed state, and their change in duration with voltage comes from the voltage dependence of the deactivation rate constant β. In our kinetic scheme the short-lived intraburst closed state is placed after the open state, though several alternatives are possible (Scheme 3), because this provides a better quantitative fit to the data and also gives a straightforward explanation for the voltage dependence of channel closing on repolarization in voltage-dependent K^+ channels.

Another characteristic feature of K_{O_2} channel gating is that they normally make several bursts during a pulse, which is interpreted to mean that the closed or inactivated states occupied after termination of the first burst are very reversible. In this respect, K_{O_2} channels differ also from native *Shaker* K^+ channels that exhibit one or two bursts per trace (Zagotta and Aldrich, 1990). Reopening, in the sense that it reflects returning to the open state from either a closed or an inactivated state, may

be a feature of voltage-gated channels depending on environmental factors (as suggested by Gonoi and Hille, 1987 in an illustrative discussion on the gating of Na^+ channels) or subtle molecular differences. These variables possibly alter the relative weight of the deactivation and inactivation rate constants, as well as the reversibility of the inactivated state, and so determine the fate of the channels after the initial opening. At the macroscopic level, these phenomena explain the variability in the inactivation time course of K^+ channels from different preparations (see Rudy, 1988, for a review).

We propose the existence of two inactivated states, or inactivating processes (Iverson and Rudy, 1990; Hoshi, Zagotta, and Aldrich, 1991). This is compatible with the fact that both macroscopic O_2-sensitive K^+ currents and ensemble average currents from patches containing only K_{O_2} channels exhibit a double exponential inactivation time course with fast and slow components. Qualitatively these components could be preferentially related to the reversible (I_0) and irreversible (I_1) inactivated states. States I_0 and I_1 may not necessarily be coupled, as they appear in our kinetic scheme, though K_{O_2} channels probably prefer to inactivate sequentially through states I_0 and I_1 since burst duration distributions were consistently best fitted by single exponential functions.

As in other voltage-gated ionic channels (Armstrong and Gilly, 1979; Bean, 1981; Horn et al., 1981; Hoshi and Aldrich, 1988; Cooper and Shrier, 1989), K_{O_2} channels can inactivate from closed states. This kinetic feature is steeply voltage dependent and more probable at negative membrane potentials. Because channels that inactivate from a closed state do not open with a long latency, it is suggested that these transitions preferentially end at the absorbing inactivated state.

Thus, K_{O_2} channels have distinct kinetic properties that suit them well for having a major role in the electrophysiology of glomus cells. As do other transient K^+ channels, K_{O_2} channels surely influence repetitive firing frequency (López-Barneo et al., 1988; López-López et al., 1989); however, they may perform a more critical task since the high probability of closed-state inactivation at negative voltages and the slow recovery from inactivation implies that in response to small depolarizations a percentage of K_{O_2} channels can accumulate in the inactivate state even before opening, which can be used as an efficient mechanism to regulate the level of excitability of glomus cells.

Low Po_2 and Channel Gating

We have shown that upon exposure to hypoxia K_{O_2} channels open more slowly, inactivate faster, and undergo closed-state inactivation more frequently. Our model suggests that low Po_2 favors the residence of the channels in the left-most closed state (C_0) and the transitions leading to the absorbing inactivated state (I_1). Voltage-dependent transitions in the opening pathway and those between the open state and the adjacent closed and inactivated states were unaltered by hypoxia.

Low Po_2 could produce a relative stabilization of state C_0 by decreasing the free energy difference that exists between states C_0 and C_1 under normoxic conditions. This would explain the slowing down of the first latency and the more apparent effect of hypoxia at moderately low depolarizations. Low Po_2 drastically reduces the relative amplitude of the slow component of inactivation, whereas the fast component

remains almost unaltered. At the single-channel level this effect is paralleled by a decrease in the number of bursts per trace. These observations can be explained by an increase in the probability of entering the absorbing state I_1 from state I_0. Low P_{O_2} does not seem to alter state I_0 or favor direct transitions from the open to the absorbing state (I_1). Thus, hypoxia could further stabilize the absorbing state or decrease the activation energy for the transitions leading to this state. This also explains the increase in the probability of blanks at low P_{O_2} since, as indicated above, direct closed to inactivated transitions appear to end at the absorbing state. Closed-state inactivation has been assumed in previous models to occur from states near the open state (see, for example, Armstrong and Gilly, 1979; Zagotta and Aldrich, 1990). In these schemes, if the closed-state inactivation rate constant (δ) increases it produces by mass action a marked acceleration of the opening kinetics. Low P_{O_2} clearly raises the probability of blanks and reduces the size of the macroscopic K^+ current while retarding channel activation and leaving unaltered transitions near the open state. For a satisfactory quantitative fit of these phenomena it is necessary to assume that the value of δ increases upon exposure to hypoxia; therefore, we propose that in K_{O_2} channels closed-state inactivation occurs from a state not adjacent to the open state. Closed-state inactivation is, however, poorly understood and a number of possible alternatives may be raised with future research.

Because hypoxia alters well-defined kinetic properties of K_{O_2} channels, one can speculate that O_2 tension may influence the structure of specific domains of the K^+ channel molecule. In this respect, it is noteworthy to stress that low P_{O_2} does not affect either single-channel conductance or the final transitions in the opening pathway, which mainly depend on structural domains probably not easily accessible to ligands or enzymes. Changes in O_2 tension may induce structural changes in one or a few more accessible amino acids, either by a direct action or through a membrane-bound enzymatic system (see Ganfornina and López-Barneo, 1991, 1992). Along with this idea, a recent report by Ruppersberg, Stocker, Pongs, Heinemann, Frank, and Koenen (1991) is particularly attractive because it shows that the redox state of cysteine residues in the NH_2 terminus influences the inactivation time course in cloned mammalian K^+ channels expressed in oocytes.

In conclusion, the changes that occur in K_{O_2} channel kinetics upon exposure to low P_{O_2} (slower activation, faster inactivation, and favored closed-state inactivation) explain the decrease in the open probability described in the preceding report (Ganfornina and López-Barneo, 1992). Given the special kinetic features of K_{O_2} channels discussed above, these changes will markedly enhance the excitability of glomus cells and increase action potential firing frequency (see López-Barneo et al., 1988; López-López et al., 1989).

The authors wish to thank Dr. L. Tabares (University of Seville) for writing the computer program used in the reconstruction of the macroscopic currents, and Drs. R. Aldrich, T. Hoshi, and W. Zagotta (Stanford University) for critically reading the manuscript.

Research was supported by a grant from the Dirección General de Investigación Científica y Técnica (PB86-0250).

Original version received 18 December 1991 and accepted version received 16 April 1992.

REFERENCES

Aldrich, R. W., D. P. Corey, and C. F. Stevens. 1983. A reinterpretation of mammalian sodium channel gating based on single channel recording. *Nature.* 306:436–441.

Armstrong, C. M., and F. Bezanilla. 1977. Inactivation of the sodium channel. II. Gating current experiments. *Journal of General Physiology.* 70:567–590.

Armstrong, C. M., and W. Gilly. 1979. Fast and slow steps in the activation of sodium channels. *Journal of General Physiology.* 74:691–711.

Bean, B. P. 1981. Sodium channel inactivation in the crayfish giant axon. Must a channel open before inactivating? *Biophysical Journal.* 35:595–614.

Colquhoun, D. 1988. Practical analysis of single channel records. *In* Microelectrode Techniques. N. B. Standen, P. T. A. Gray, and M. J. Whitaker, editors. The Company of Biologists Ltd., Cambridge, UK. 83–104.

Colquhoun, D., and A. G. Hawkes. 1983. The principles of the stocastic interpretation of ion channel mechanisms. *In* Single Channel Recording. B. Sakmann and E. Neher, editors. Plenum Publishing Corp., New York. 135–175.

Colquhoun, D., and F. J. Sigworth. 1983. Fitting and statistical analysis of single channel records. *In* Single Channel Recording. B. Sakmann and E. Neher, editors. Plenum Publishing Corp., New York. 191–263.

Cooper, E., and A. Shrier. 1989. Inactivation of A currents and A channels on rat nodose neurons in culture. *Journal of General Physiology.* 94:881–910.

Delpiano, M. A., and J. Hescheler. 1989. Evidence for a P_{O_2}-sensitive K^+ channel in the type I cell of the rabbit carotid body. *FEBS Letters.* 249:195–198.

Duchen, M. R., K. W. T. Caddy, G. C. Kirby, D. L. Patterson, J. Ponte, and T. J. Biscoe. 1988. Biophysical studies of the cellular elements of the rabbit carotid body. *Neuroscience.* 26:291–311.

Ganfornina, M. D., and J. López-Barneo. 1991. Single K^+ channels in membrane patches of arterial chemoreceptor cells are modulated by O_2 tension. *Proceedings of the National Academy of Sciences, USA.* 88:2927–2930.

Ganfornina, M. D., and J. López-Barneo. 1992. Potassium channel types in arterial chemoreceptor cells and their selective modulation by oxygen. *Journal of General Physiology.* 100:401–426.

Gonoi, T., and B. Hille. 1987. Gating of Na channels. Inactivation modifiers discriminate among models. *Journal of General Physiology.* 89:253–274.

Hamill, O. P., A. Marty, E. Neher, B. Sakmann, and F. J. Sigworth. 1981. Improved patch-clamp techniques for high-resolution current recording from cells and cell-free membrane patches. *Pflügers Archiv.* 391:85–100.

Hescheler, J., M. A. Delpiano, H. Acker, and F. Pietruschka. 1989. Ionic currents on type I cells of the rabbit carotid body measured by voltage-clamp experiments and the effect of hypoxia. *Brain Research.* 486:79–88.

Horn, R. 1987. Statistical methods for model discrimination. Applications to gating kinetics and permeation of the acetylcholine receptor channel. *Biophysical Journal.* 51:255–263.

Horn, R., J. Patlak, and C. F. Stevens. 1981. Sodium channels need not open before they inactivate. *Nature.* 291:426–427.

Hoshi, T., and R. W. Aldrich. 1988. Gating kinetics of four classes of voltage-dependent K^+ channels in pheochromocytoma cells. *Journal of General Physiology.* 91:107–131.

Hoshi, T., W. N. Zagotta, and R. W. Aldrich. 1991. Two types of inactivation in *Shaker* K^+ channels: effects of alterations in the carboxyl terminal region. *Neuron.* 7:547–556.

Iverson, L. E., and B. Rudy. 1990. The role of the divergent aminoacid and carboxyl domains on the inactivation properties of potassium channels derived from the *Shaker* gene of *Drosophila*. *Journal of Neuroscience.* 10:2903–2916.

Kirsch, G. E., and A. M. Brown. 1989. Kinetic properties of single sodium channels in rat heart and rat brain. *Journal of General Physiology.* 93:85–99.

Levitan, I. B. 1988. Modulation of ion channels in neurons and other cells. *Annual Review of Neuroscience.* 11:119–136.

López-Barneo, J., J. R. López-López, J. Ureña, and C. González. 1988. Chemotransduction in the carotid body: K^+ current modulated by P_{O_2} in type I chemoreceptor cells. *Science.* 241:580–582.

López-López, J. R., C. González, J. Ureña, and J. López-Barneo. 1989. Low P_{O_2} selectively inhibits K^+ channel activity in chemoreceptor cells of the mammalian carotid body. *Journal of General Physiology.* 93:1001–1015.

Magleby, K. L., and B. S. Pallota. 1983. Burst kinetics of single calcium-activated potassium channels in cultured rat muscle. *Journal of Physiology.* 344:605–623.

Patlak, J., and R. Horn. 1982. Effect of N-bromoacetamide on single sodium channel currents in excised membrane patches. *Journal of General Physiology.* 79:333–351.

Perozo, E., D. S. Jong, and F. Bezanilla. 1991. Single-channel studies of the phosphorylation of K^+ channels in the squid giant axon. *Journal of General Physiology.* 98:19–34.

Rudy, B. 1988. Diversity and ubiquity of K channels. *Neuroscience.* 25:729–749.

Ruppersberg, J. P., M. Stocker, O. Pongs, S. H. Heinemann, R. Frank, and M. Koenen. 1991. Regulation of fast inactivation of cloned mammalian I_k(A) channels by cysteine oxidation. *Nature.* 352:711–714.

Solc, C. K., and R. W. Aldrich. 1990. Gating of single non-*Shaker* A-type potassium channels in larval *Drosophila* neurons. *Journal of General Physiology.* 96:135–165.

Stea, A., and C. A. Nurse. 1991. Whole-cell and perforated-patch recordings from O_2-sensitive rat carotid body cells grown in short- and long-term culture. *Pflügers Archiv.* 418:93–101.

Ureña, J., J. R. López-López, C. González, and J. López-Barneo. 1989. Ionic currents in dispersed chemoreceptor cells of the mammalian carotid body. *Journal of General Physiology.* 93:979–999.

Zagotta, W. N., and R. W. Aldrich. 1990. Voltage-dependent gating of *Shaker* A-type potassium channels in *Drosophila* muscle. *Journal of General Physiology.* 95:29–60.